Final Project: System Identification Techniques

MAE 283A: Professor Raymond de Callafon

Shivharsh Kand

Background:

In this project, I modelled the dynamics of a self-sustaining power grid or more specifically, Kaiser Microgrid. Additionally, the data set that I used was specifically, the random excitation of the real power demand of the inverter with measurements from the real power at the Battery Energy Storage System (BESS). I would like to thank Professor De Callafon and System Identification and Control Laboratory for providing me with this test data.

1. Non-Parametric Identification:

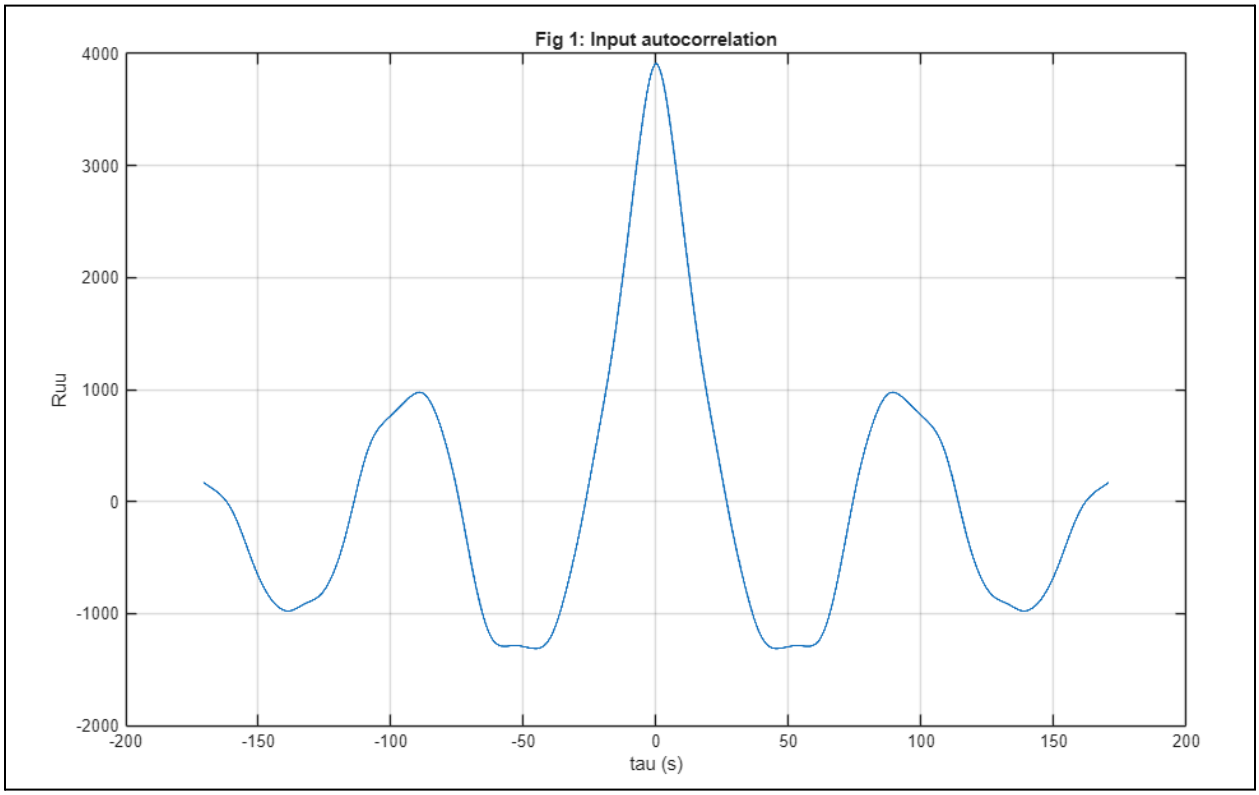

Figure 1: Highlights the estimated input autocorrelation function.

Figure 1 delineates a significant correlation for non-zero lags. This indicates that the input used for this system was not white noise. The oscillation seen can hint towards a low-frequency dominated signal which might be produced by a slow and varying excitation, something that is typically seen with power-electronic systems (in this case BESS).

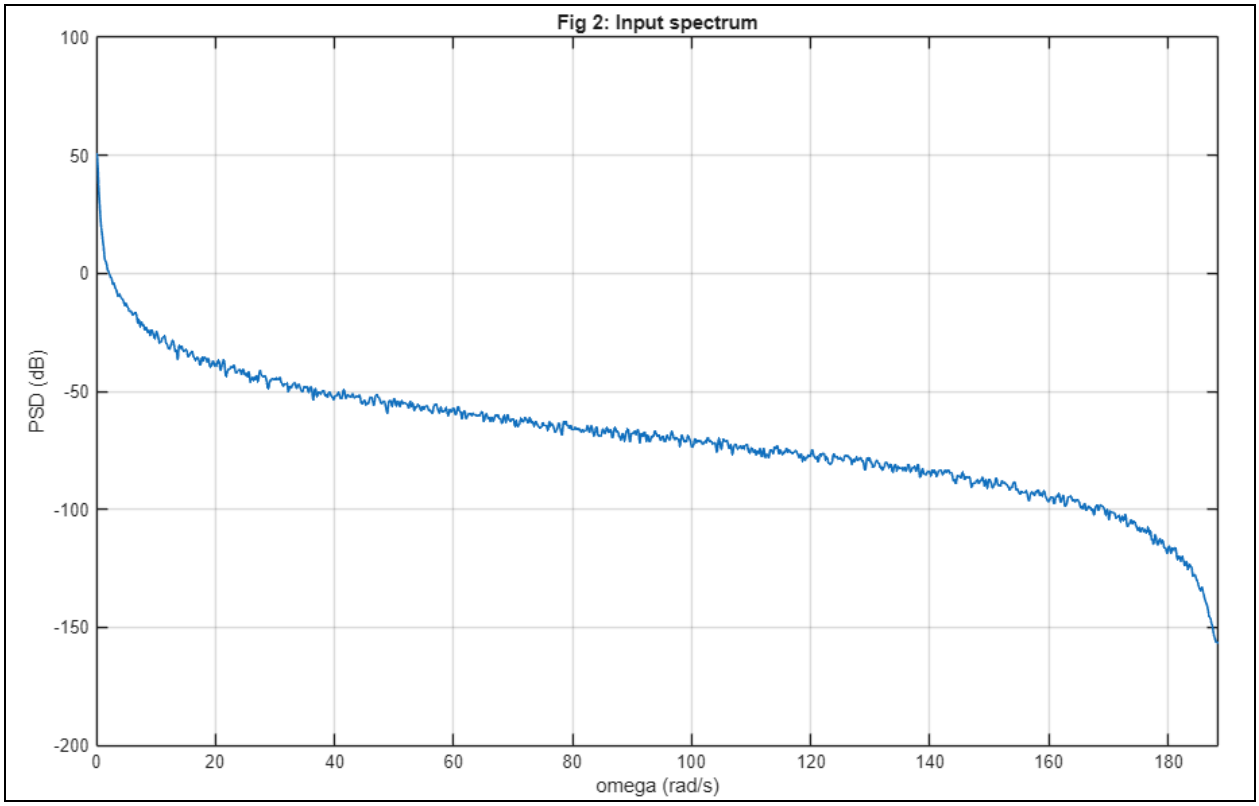

Figure 2: Highlights the estimated Input Spectrum

Figure 2 highlights that the input spectrum (plotted in dB) is concentrated at low frequencies, meaning that the input is strongly excited at low frequencies and weakly excited at high frequencies. As a result, the spectral estimate of the frequency response $G_0(e^{jw})$ will be reliable over the low-frequency range, primarily because the input signal will have sufficient power.

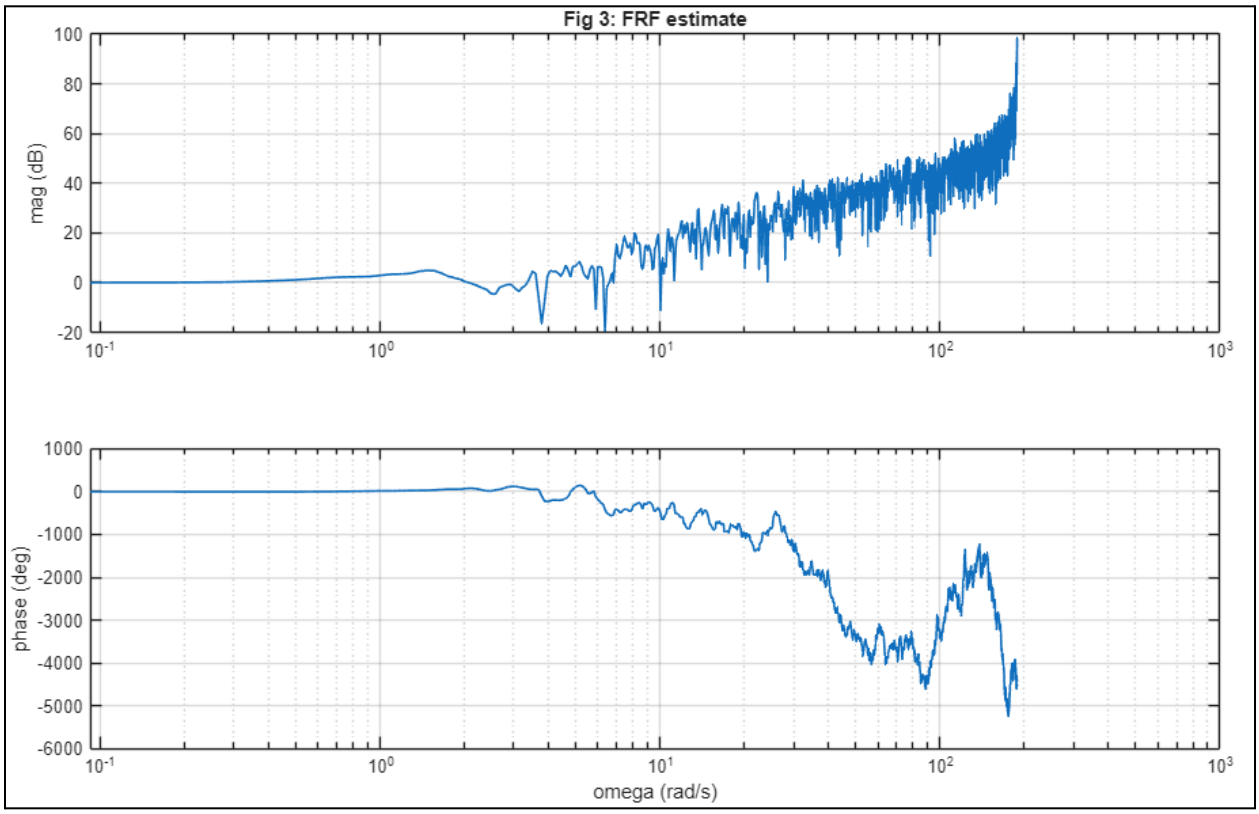

Figure 3: Highlights Bode Plot of the SPA estimate of the System Frequency Response

Figure 3 delineates Bode plot of the spectral estimate of the system frequency response. The estimate was obtained using windowed and averaged periodogram-based spectral analysis, following the approach discussed in lecture. In practice, a Hann window was applied to each data segment before averaging the periodograms which helped reduce variance in the spectral estimate.

With regards to Figure 2 and 3, the input signal excites the system at low frequencies as the input spectrum decays significantly at higher frequencies. We can see this from the bode plots as the lower frequencies depict a more reliable response with almost no variance. However at higher frequencies we see increased variance, primarily due to limited excitation. Therefore, this suggests that downsampling the input-data, by increasing ΔT will be beneficial, as the system dynamics, in this particular case, are low-frequency dominated.

2. Parametric Identification:

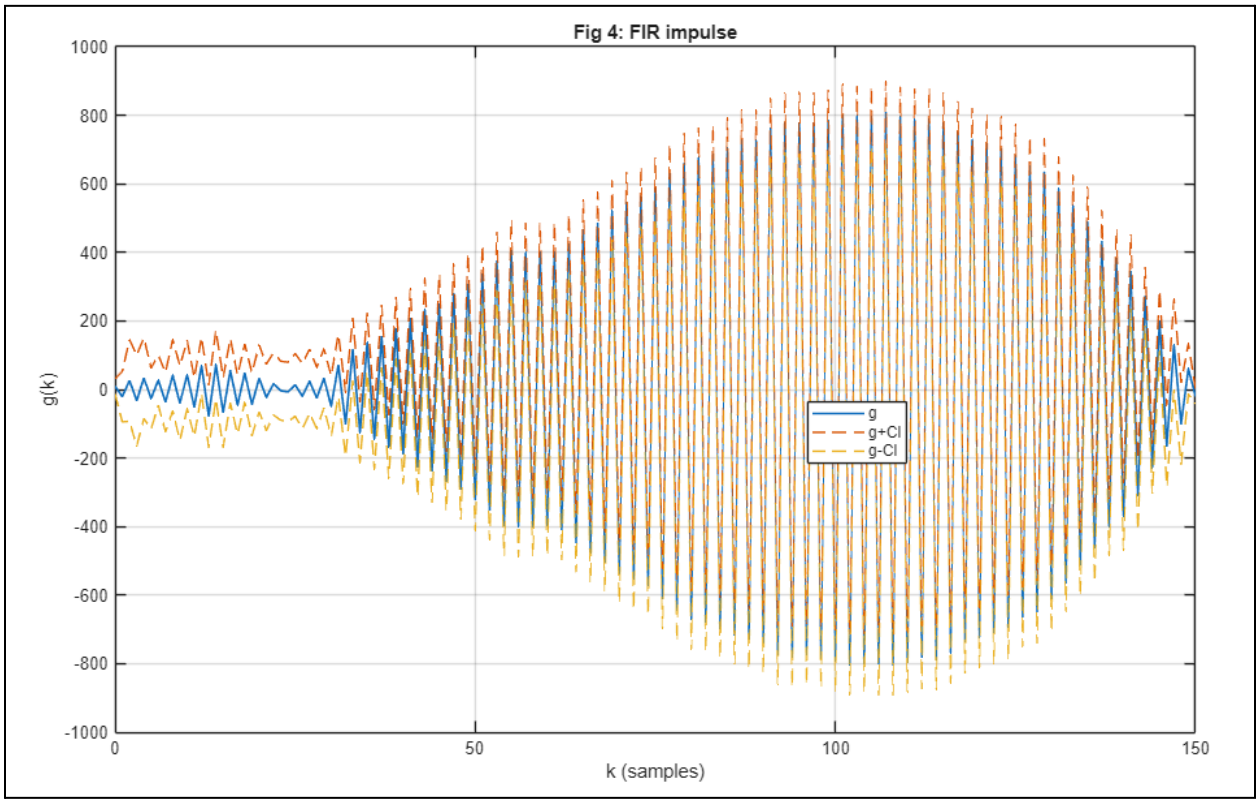

Figure 4: Highlights the estimated impulse response parameters

Figure 4 depicts the estimated FIR impulse response coefficients, along with the corresponding 99% confidence bounds. The FIR order for this part was chosen as n = 150. This order ensures that the dominant impulse response dynamics are captured before the coefficients decay to zero while remaining below the N/10 factor to limit noise amplification. Through this estimate, we can see that there is an oscillatory behavior along with slow decay, hinting at a long memory dynamics in this system. We can also see that the confidence bounds increase for larger values of k which show that there is an increase in the uncertainty of the estimates as the input signal is not white.

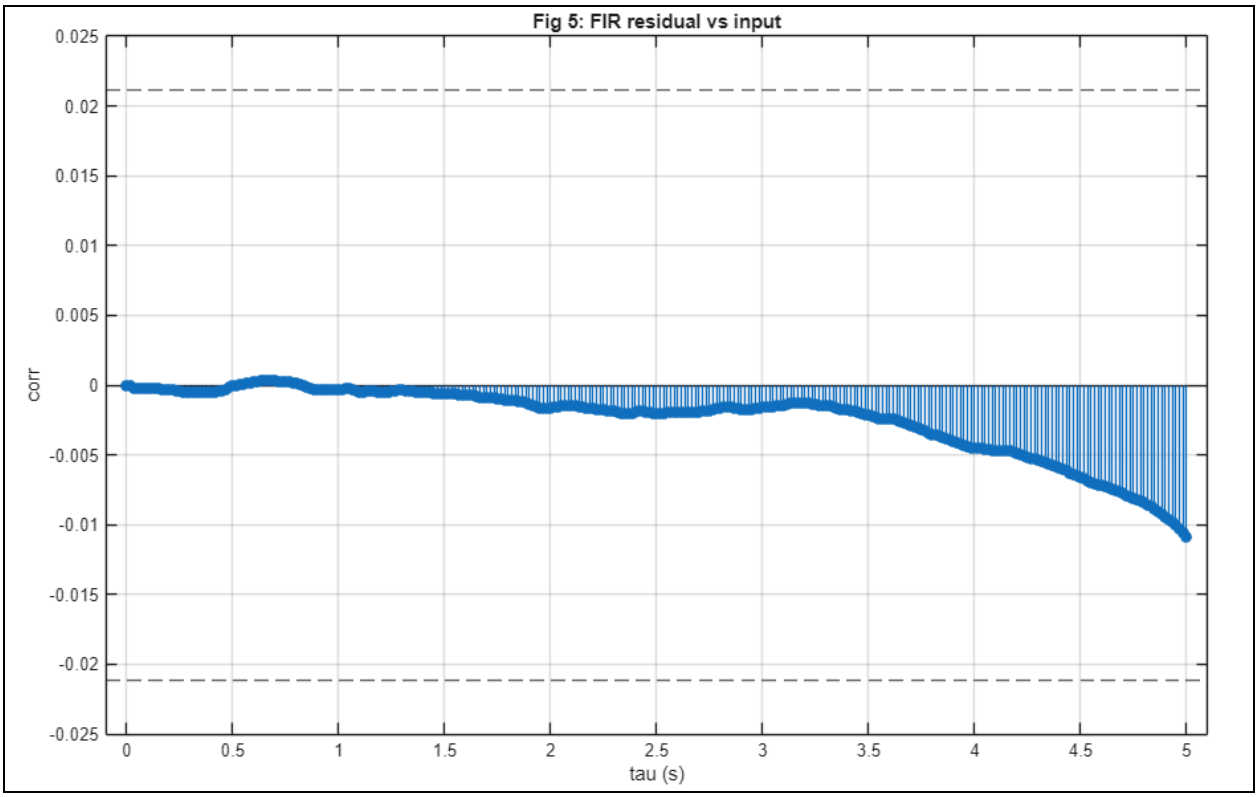

Figure 5: Highlights the estimated cross-correlation function between FIR Residual and Input

Figure 5 depicts the estimated cross-correlation function between the FIR residual and the input, along with the fixed 99% confidence bounds. Although there is a subtle systematic trend seen at larger lags, the correlation between the two remains within the confidence bounds for all $0 \leq \tau \leq 2n$. Therefore, this particular FIR model passes the model validation test with 99% probability. Finally, as there is no significant correlation between the FIR residual and the input at small positive lags, therefore any pure time delay in the system is negligible relative to the sampling time.

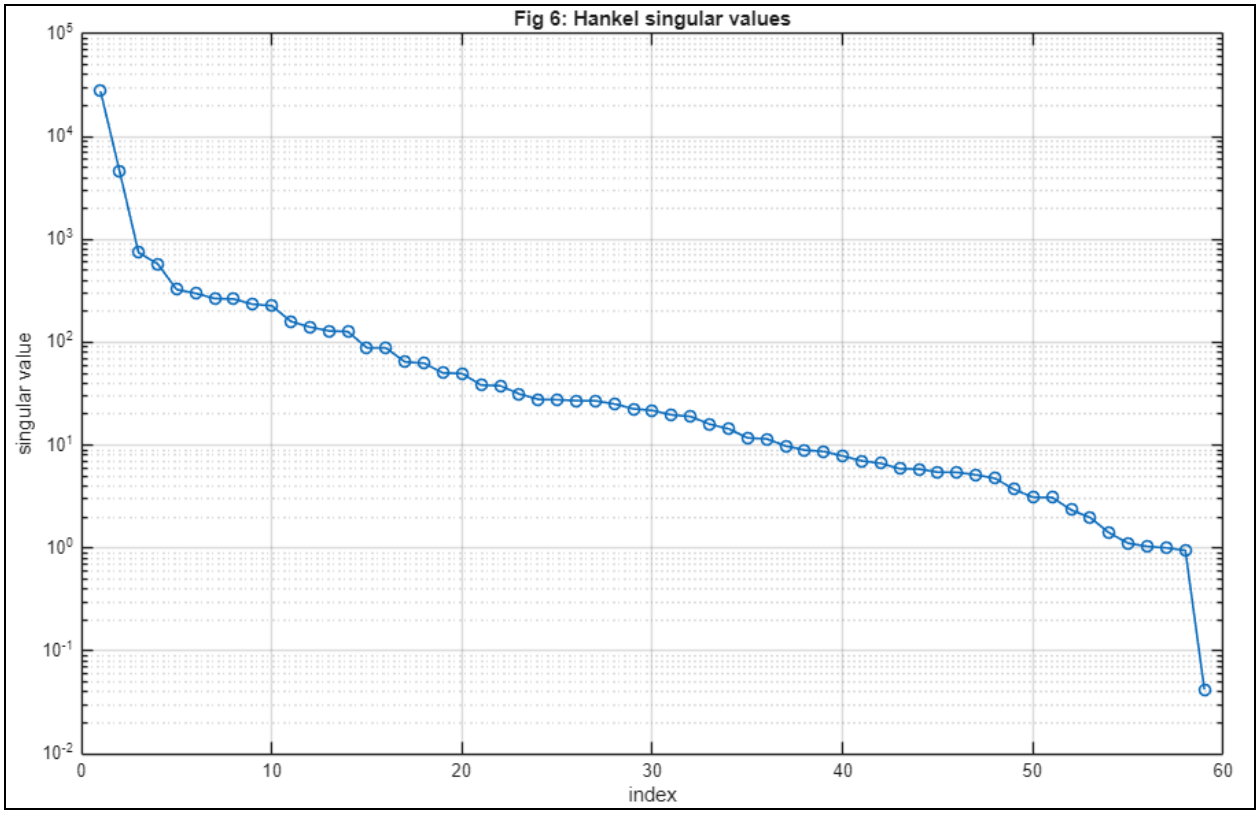

Figure 6: Highlights Hankel Singular Values for Model Order Selection

Figure 6 depicts the Hankel singular values obtained from the realization algorithm. Rapid decay is seen over the first few indices and then there is a gradual decrease for the higher order modes. Keeping this in mind the state space model order can be from n = 3 to 6, as this provides a reasonable compromise between model complexity and fidelity.

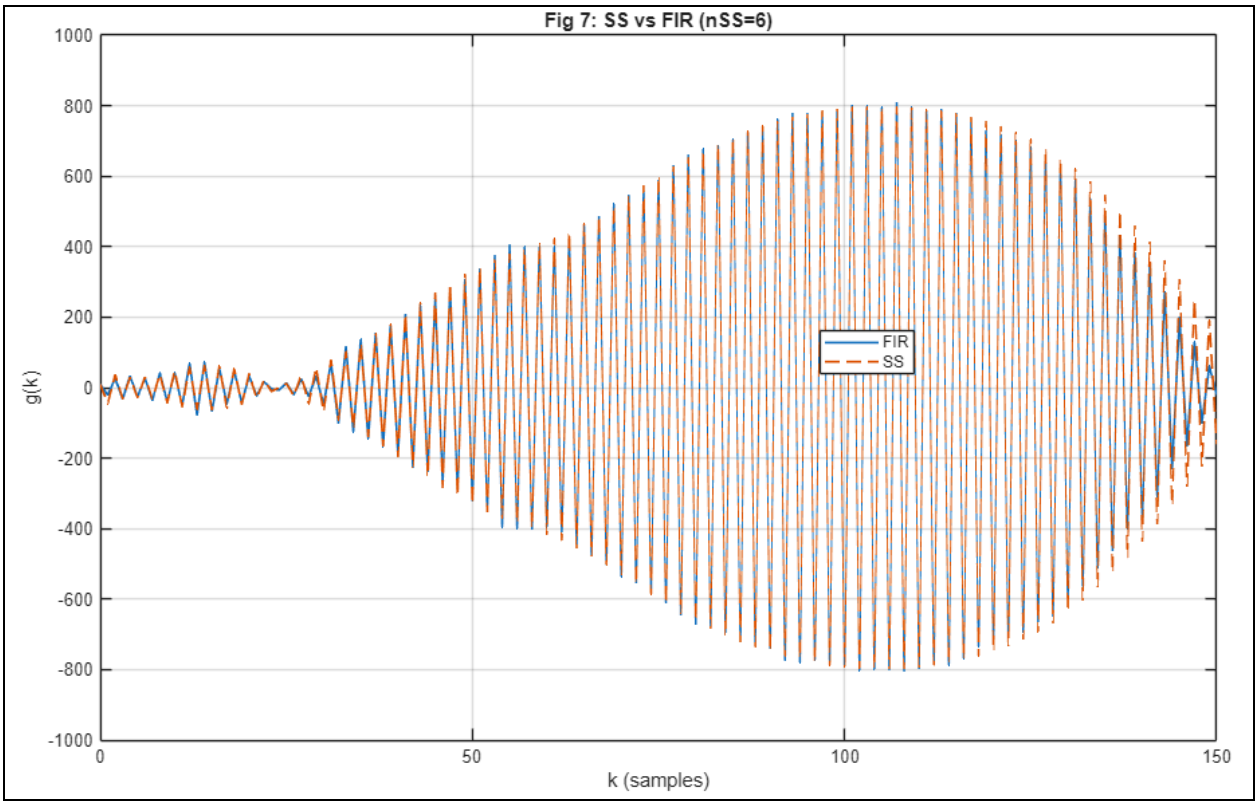

Figure 7: Comparison between FIR and SS Model

Figure 7 shows the impulse response of the estimated state-space model obtained via the realization algorithm. For comparison, the impulse response estimated from the FIR model is also shown. In terms of the accuracy, the state space impulse response shows good agreement with the FIR impulse response. However, at larger time indices, we see minor discrepancies due to noise effect and truncation that comes along with the chosen state dimension.

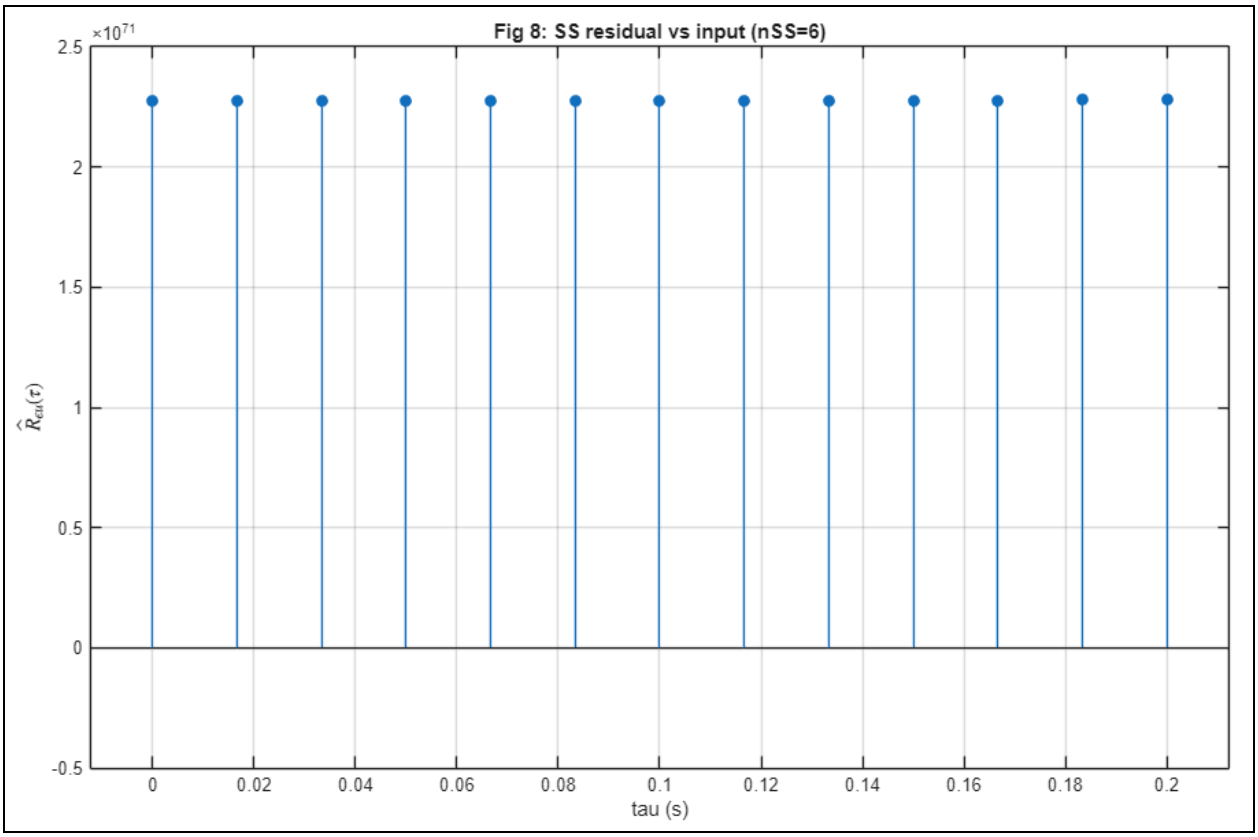

Figure 8: Highlights the estimated cross-correlation between the input and the simulation error of the SS-Model

Figure 8 delineates that the cross-correlation estimated is clearly nonzero over the range $0 \leq \tau \leq 2n$ and lies far outside the fixed 99% confidence bounds. This indicates clearly that the simulation error is strongly correlated with the input signal. Additionally, the large magnitude reflects numerical scaling of the correlation estimate. Keeping this in mind, the state space model fails the model validation test. The lag axis is shown in seconds, where the maximum lag corresponds to 2n samples multiplied by the sampling period.

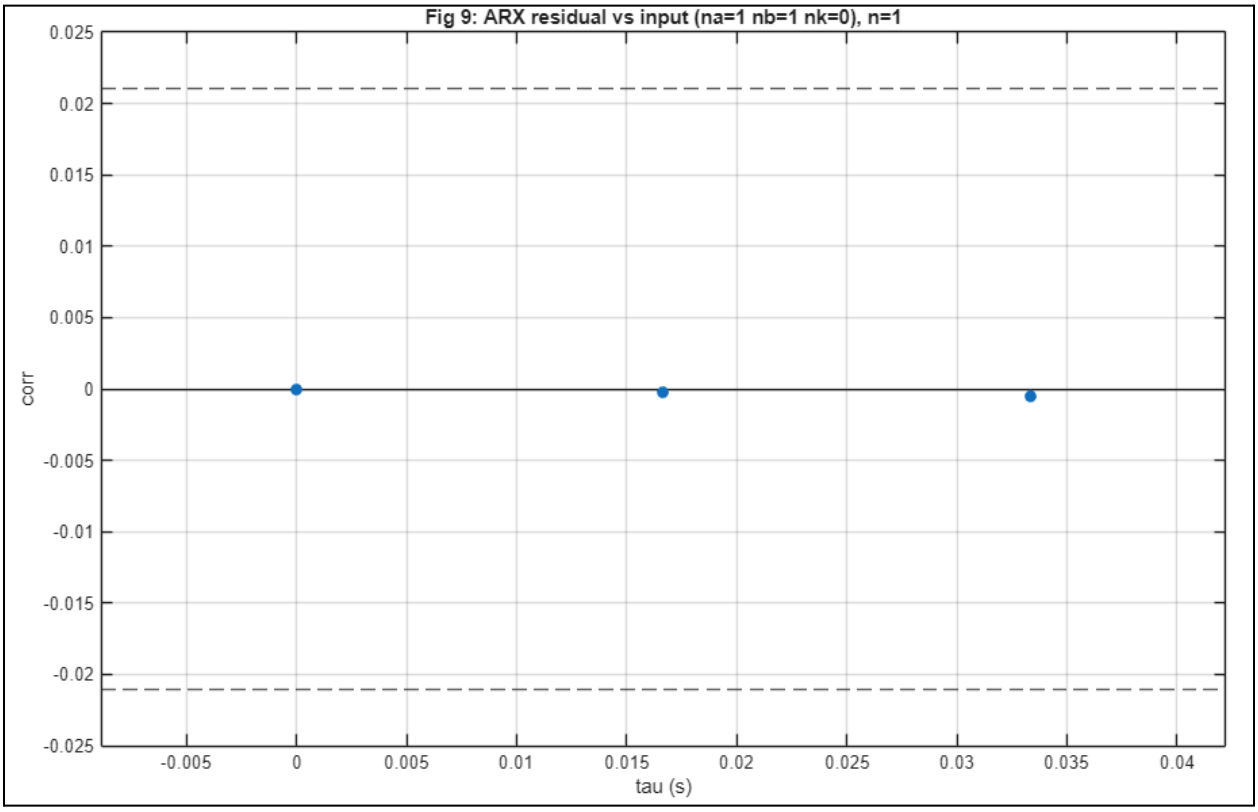

Figure 9: Highlights the ARX Model

Figure 9 depicts the cross-covariance function along with the 99% confidence bounds. This figure highlights the that the chosen ARX model with $n_a = 1, n_b = 1, n_c = 0$, satisfies the model validation criterion. Additionally, this chosen model is the lowest-order structure that yields residuals which are uncorrelated with the input within the 99% confidence bounds.

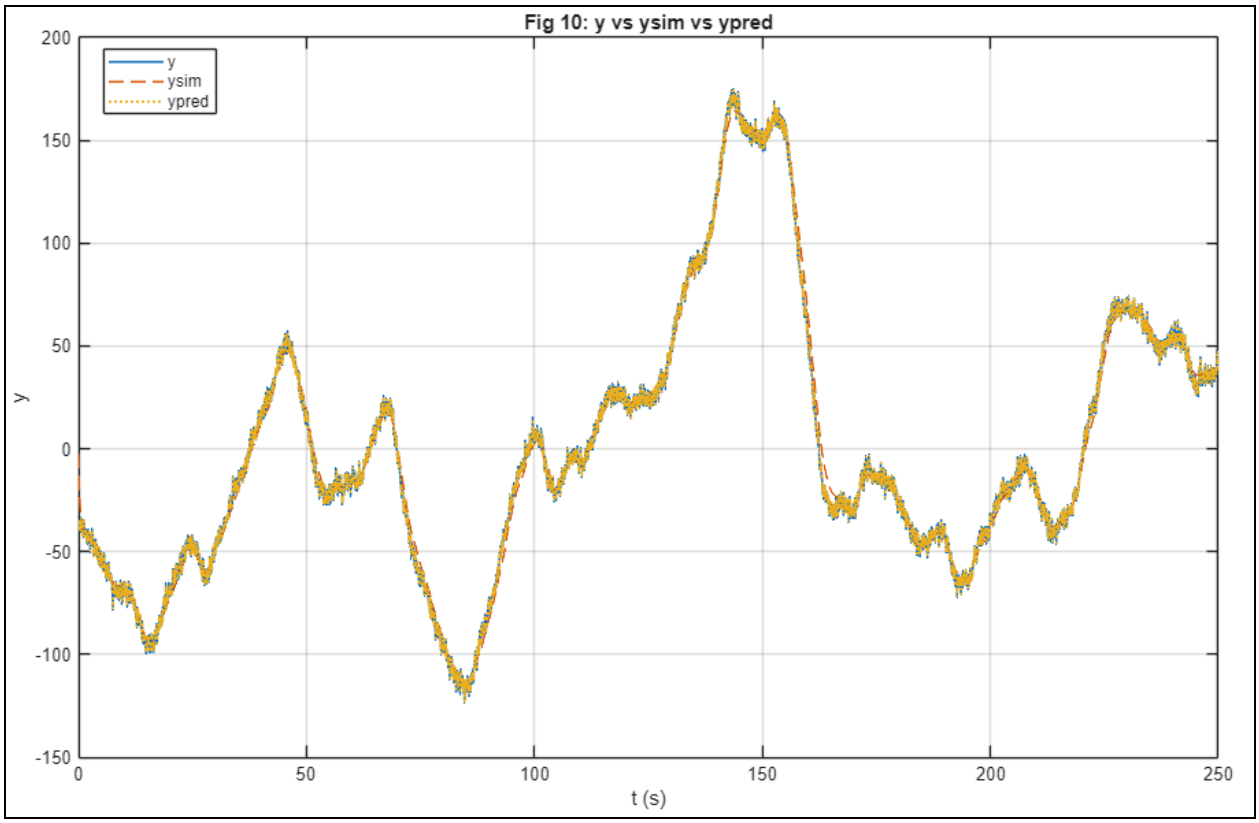

Figure 10: Simulation VS Prediction performance

Figure 10 compares the measured output of the system y(t) with the simulated output y_sim(t) and the one-step-ahead predicted output y_pred(t). From the graph, it can be seen that the predicted output follows the measured output closely over the entire time interval. This highlights that the model accurately captures the input-output dynamics of the system when past output information is used. While the simulated output is also quite successful in tracking the overall system behaviour, it definitely exhibits larger deviations in comparison to the predicted output. This difference between the two is expected as simulation relies solely on the input and the accumulated system dynamics. Overall, I believe that the results indicate good predictive and satisfactory simulation performance for the chosen low-order ARX model.